The Plant Journal, volume 111, pages 205-216 (2022)
https://doi.org/10.1111/tpj.15787

The endoplasmic reticulum membrane–bending protein RETICULON facilitates chloroplast relocation movement in *Marchantia polymorpha*

Kazuya Ishikawa[1], Ryota Konno[1], Satoyuki Hirano[1], Yuta Fujii[1], Masayuki Fujiwara[2,3], Yoichiro Fukao[2,4], and Yutaka Kodama[1,*]

[1]Center for Bioscience Research and Education, Utsunomiya University, Tochigi, Japan
[2]Plant Global Education Project, Graduate School of Biological Sciences, Nara Institute of Science and Technology, Nara, Japan
[3]YANMAR HOLDINGS Co. Ltd., Osaka, Japan
[4]Department of Bioinformatics, College of Life Sciences, Ritsumeikan University, Shiga, Japan

[*]Corresponding Author: e-mail: Yutaka Kodama
kodama@cc.utsunomiya-u.ac.jp

SUMMARY
Plant cells alter the intracellular positions of chloroplasts to ensure efficient photosynthesis, a process controlled by the blue light receptor phototropin. Chloroplasts migrate towards weak light (accumulation response) and move away from excess light (avoidance response). Chloroplasts are encircled by the endoplasmic reticulum (ER), which forms a complex network throughout the cytoplasm. To ensure rapid chloroplast relocation, the ER must alter its structure in conjunction with chloroplast relocation movement, but little is known about the underlying mechanism. Here, we searched for interactors of phototropin in the liverwort *Marchantia polymorpha* and identified a RETICULON (RTN) family protein; RTN proteins play central roles in ER tubule formation and ER network maintenance by stabilizing the curvature of ER membranes in eukaryotic cells. *Marchantia polymorpha* RTN1 (MpRTN1) is localized to ER tubules and the rims of ER sheets, which is consistent with the localization of RTNs in other plants and heterotrophs. The Mp*rtn1* mutant showed an increased ER tubule diameter, pointing to a role for MpRTN1 in ER membrane constriction. Furthermore, Mp*rtn1* showed a delayed chloroplast avoidance response but a normal chloroplast accumulation response. Live-cell imaging of ER dynamics revealed that ER restructuring was impaired in Mp*rtn1* during the chloroplast avoidance response. These results suggest that during the chloroplast avoidance response, MpRTN1 restructures the ER network and facilitates chloroplast movement via an interaction with phototropin. Our findings provide evidence that plant cells respond to fluctuating environmental conditions by controlling the movements of multiple organelles in a synchronized manner.

KEY WORDS: chloroplast relocation; phototropin; endoplasmic reticulum; RETICULON; *Marchantia polymorpha*

SIGNIFICANCE STATEMENT
Although chloroplasts are encircled by the endoplasmic reticulum (ER), they move rapidly within a cell in response to light to ensure efficient photosynthesis, but the regulatory mechanism of ER structure during chloroplast movement remains unknown. Here, we reveal that in *Marchantia polymorpha*, the blue light receptor phototropin, which mediates chloroplast movement, interacts with an ER membrane-bending protein reticulon (MpRTN1), and that MpRTN1 restructures the ER network and facilitates phototropin-mediated chloroplast movement.

INTRODUCTION

Chloroplasts alter their intracellular positions to achieve efficient photosynthesis under variable light conditions (Wada, 2013). Specifically, chloroplasts accumulate along the periclinal cell wall under low-light conditions (accumulation response) and move toward the anticlinal cell walls under high-light conditions (avoidance response). As the temperature decreases, the cellular sensitivity to light changes, and chloroplasts show an avoidance response even under low-light conditions (cold-avoidance response) (Kodama *et al.*, 2008). All three types of chloroplast relocation are regulated by the blue light receptor phototropin (phot) (Jarillo *et al.*, 2001; Kagawa *et al.*, 2001; Sakai *et al.*, 2001), with the support of several regulatory proteins localized to the plasma membrane, the chloroplast outer envelope, actin filaments, and the cytosol (Suetsugu *et al.*, 2010; Kodama *et al.*, 2010; Oikawa *et al.*, 2008). In Arabidopsis (*Arabidopsis thaliana*), two phots (phot1 and phot2) transduce the signal generated through the perception of blue light to regulatory proteins and reorganize actin filaments associated with chloroplasts, providing the driving force for chloroplast relocation movement (Suetsugu and Wada, 2020). Some regulatory proteins have been reported to be phosphorylated, and the phosphorylation is believed to be the identity of the signal.

The endoplasmic reticulum (ER) forms a complex network in plant cells. Most of the volume of a mature plant cell is occupied by the vacuole, whereas the ER and other organelles are densely packed in a thin layer between the plasma membrane and tonoplast (Winter *et al.*, 1994). Therefore, the ER closely interacts with other organelles both physiologically and functionally (Prinz *et al.*, 2020). The cortical ER underneath the plasma membrane is in physical contact with the plasma membrane at subdomains known as ER–plasma membrane contact sites (Ishikawa *et al.*, 2018; Ishikawa *et al.*, 2020), which are thought to function in cell signaling and lipid transport (Wang *et al.*, 2017). Furthermore, the ER network surrounds and makes physical contact with chloroplasts, presumably to exchange lipid molecules (Block and Jouhet, 2015). Indeed, several confocal microscopy studies have revealed ER tubules encircling the chloroplasts in Arabidopsis cells (Nziengui *et al.*, 2007; Andersson *et al.*, 2007). When chloroplasts relocate in plant cells, the ER must alter its morphology to maintain the ER-chloroplast interaction and avoid blocking chloroplast movement. However, to the best of our knowledge, no studies have reported the relationship between ER structure and chloroplast relocation movement.

ER morphology and the ER network are maintained by the cytoskeleton and integral membrane proteins that shape ER membrane curvature (Zhang and Hu, 2016). Members of the ER integral protein family RETICULON (RTN) function in ER tubule formation, cortical network maintenance (Voeltz *et al.*, 2006), and stress responses (Zhang *et al.*, 2020; Huang and Hwang, 2020). Arabidopsis has 21 *RTN* genes (At*RTNs*), which are phylogenetically clustered into three major groups (RTN clusters 1–3) (Nziengui *et al.*, 2007). Although the functional analysis is difficult due to the high genetic redundancy, the overexpression of RTNs belonging to cluster 1 induced ER tubule constriction (Tolley *et al.*, 2008b; Sparkes *et al.*, 2010; Kriechbaumer *et al.*, 2018; Lazareva *et al.*, 2021), pointing to the membrane-bending activity of these proteins in plant cells.

Marchantia (*Marchantia polymorpha*) is a basal land plant that is attracting increasing attention as a model plant. Marchantia is highly compatible with molecular genetics because of its low genetic redundancy and haploidy in addition to the ease of growth and transformation (Bowman et al., 2017). Marchantia has a single *PHOTOTROPIN* gene,

whose protein product mainly localizes at the plasma membrane and controls chloroplast relocation in a blue light-dependent manner, similar to angiosperms (Komatsu *et al.*, 2014; Fujii *et al.*, 2017; Fujii *et al.*, 2020; Hirano *et al.*, 2022). In this study, we identified an RTN (MpRTN1) as an interactor of Marchantia phot (Mpphot). In Marchantia, Mp*RTN1* is the only gene belonging to the RTN clusters 1, and a mutant defective in Mp*RTN1* showed reduced constriction of ER tubules and a delayed chloroplast avoidance response. Live-cell imaging of ER dynamics revealed that ER restructuring during the avoidance response was impaired in the MpRTN1-deficient mutant. These findings suggest that MpRTN1 facilitates the chloroplast avoidance response in coordination with Mpphot by adjusting ER structure to assist chloroplast relocation movement.

RESULTS

Mpphot interacts with MpRTN1

To identify interactors of Mpphot, we performed an immunoprecipitation assay using wild-type (WT) Marchantia plants and transgenic Marchantia plants expressing Mpphot-Citrine or free Citrine. We analyzed the immunoprecipitates by mass spectrometry and identified candidate Mpphot interactors that were specifically detected in the Mpphot-Citrine precipitate (Fig. 1A). Of these candidates, we focused on MpRTN1 because a previous interactome study of AtRTNs suggested that phot1 (Atphot1) interacts with AtRTN3 and AtRTN6 in Arabidopsis (Kriechbaumer *et al.*, 2015). To confirm the interaction between Mpphot and MpRTN1, we performed a co-immunoprecipitation assay using *Nicotiana benthamiana* leaves transiently expressing Mpphot-3xFLAG with MpRTN1-GFP or GFP fused with ER-targeting signal sequences (er-GFP) for the control. MpRTN1-GFP was detected in the precipitate of Mpphot-3xFLAG, but er-GFP was not (Fig. 1B). Although only a small proportion of MpRTN1-GFP was precipitated by Mpphot-3xFLAG (Fig. 1B, left middle panel), a longer exposure time clearly identified MpRTN1-GFP in the precipitate (Fig. 1B, right panel).

To verify the interaction between Mpphot and MpRTN1 in vivo, we performed YFP-based bimolecular fluorescence complementation (BiFC) analysis. As a plasma membrane protein Mpphot and a putative ER membrane protein MpRTN1 are likely to interact at ER-plasma membrane contact sites, we used Arabidopsis synaptotagmin 1 (AtSYT1), an ER-plasma membrane tethering factor that was previously reported to form homodimers (Ishikawa *et al.*, 2020), as a positive control. Clear dotted-line-like YFP signals were observed on the plasma membrane when AtSYT1 fused with the N-terminal half of YFP (AtSYT1-NY) and AtSYT1 fused with the C-terminal half of YFP (AtSYT1-CY) were transiently co-expressed in *N. benthamiana* leaves (Figure 1C). Similarly, dotted-line-like YFP signals were observed on the plasma membrane when a pair of Mpphot-NY and MpRTN1-CY or MpRTN-NY and Mpphot-CY were co-expressed (Figure 1C). Conversely, only relatively weak fluorescent signals were observed when Mpphot-NY or MpRTN1-NY was co-expressed with free CY (Figure 1C). These findings suggest that Mpphot interacts with MpRTN1 at ER-plasma membrane contact sites.

As phot has a kinase domain and transduces the blue light signal to several interactors via phosphorylation (Demarsy *et al.*, 2012; Takemiya *et al.*, 2013), we examined whether MpRTN1 is phosphorylated by Mpphot in Marchantia plants. WT and Mpphot knockout plants (Mp*phot*^{KO}) were irradiated with blue light and analyzed by immunoblot analysis using anti-MpRTN1 antibody and Phos-tag SDS-PAGE (Kinoshita *et al.*, 2009; Kinoshita

et al., 2012). No mobility shift of MpRTN1 was detected at any Phos-tag concentration (Fig. S1A and S1B), suggesting that MpRTN1 is not phosphorylated by Mpphot.

Phylogenetic analysis of Marchantia RTNs

As the biological functions of Marchantia RTNs have not been reported, we investigated *RTN* genes in the Marchantia genome. Sequence homology searches using a genome database for *M. polymorpha* revealed at least five *RTN* genes in the Marchantia genome (Mp*RTN1–5*), implying the lower functional redundancy of *RTN* genes than in Arabidopsis. Mp*RTN1–4* are ubiquitously expressed based on previous transcriptome analysis (Fig. S2; Bowman et al., 2017). Similarly, Mp*RTN5* is expressed in various organs but is not significantly expressed in sporelings. To gain insights into the functional differentiation of these Marchantia *RTNs*, we constructed a phylogenetic tree of Arabidopsis and Marchantia RTNs. The RTNs were clustered into three clades (Fig. 2), which is consistent with the previously reported phylogenetic relationships of At*RTNs* (Nziengui *et al.*, 2007). Mp*RTN1* and *3* were classified into clades 1 and 2, respectively, and Mp*RTN4* and *5* were classified into clade 3 (Fig. 2). Mp*RTN2* has diverged from a common ancestral gene of clade 1 (Fig. 2).

Arabidopsis and Marchantia RTNs in clade 1 range from 162 to 271 amino acids long and were predicted to contain only an RTN domain (Fig. 2 and S2). Clade 2 RTNs are approximately 560 amino acids long, with an N-terminal region that was predicted to contain a 3-beta hydroxysteroid dehydrogenase/isomerase family domain in addition to the RTN domain (Fig. 2 and 2S). Clade 3 RTNs (excluding MpRTN5) range from 431 to 640 amino acids long and, like clade 2 RTNs, contain an additional N-terminal region; however, no conserved domain was predicted in this N-terminal region (Fig. 2 and S2). MpRTN2 and 5 are shorter than other RTNs in clades 1 and 3 due to the lack of N-terminal extensions (Fig. S2), pointing to the functional differentiation of these MpRTNs. Collectively, the phylogenetic clustering and conserved domain structure of MpRTN1 with Arabidopsis clade 1 RTNs, whose overexpression leads to the constriction of ER tubules (Tolley *et al.*, 2008b; Sparkes *et al.*, 2010; Kriechbaumer *et al.*, 2018), imply that MpRTN1 is responsible for ER membrane curvature in Marchantia.

Generation of a mutant defective in Mp*RTN1* by CRISPR-Cas9-mediated genome editing

To analyze the biological function of Mp*RTN1*, we generated a Marchantia mutant defective in Mp*RTN1* by CRISPR (clustered regularly interspaced short palindromic repeats)-Cas9-mediated genome editing. We successfully established a mutant line in which a 1-bp deletion was introduced 28 bp downstream of the transcription start site of Mp*RTN1* (Fig. 3A). Although we obtained several independent gene-edited lines across multiple biological replicates, all the lines had the same mutation (1-bp deletion 28 bp downstream of the start codon). The Mp*rtn1* mutant displayed growth defects in gemmalings at the early stages of development (Fig. 3B and 3C). The growth defects were rescued by the expression of MpRTN1-Citrine (Compl), suggesting they were caused by the mutation in Mp*RTN1*. Immunoblot analysis revealed that a truncated form of MpRTN1 was expressed in Mp*rtn1* but at a level significantly lower than that of the intact protein in the WT (Fig. 3D). This truncated form of MpRTN1 was likely translated from the in-frame ATG start codon that formed due to the 1-bp deletion (Fig. 3A). Given that no mutations other than the 1-bp deletion at 28 bp were introduced by the CRISPR-

Cas9 system, perhaps mutations that knock out Mp*RTN1* are lethal or cause severe growth defects that prohibit the establishment of gene-edited lines.

MpRTN1 localizes to ER tubules and the rims of ER sheets to constrict the membrane

To investigate the subcellular localization of MpRTN1, we generated a transgenic Marchantia line coexpressing MpRTN1-Citrine and ER-targeted mCherry (er-mCherry) in the Mp*rtn1* background. A large fraction of MpRTN1-Citrine localized to ER tubules and the rims of ER sheets (Fig. 4A), whereas a small fraction of MpRTN1-Citrine localized inside the ER sheets (Fig. 4B). This observation is consistent with the finding that RTNs preferentially localize to regions of high membrane curvature (Voeltz *et al.*, 2006; Kiseleva *et al.*, 2007).

To analyze the role of MpRTN1 in regulating ER morphology, we observed the cortical ER (visualized with er-mCherry) in the WT, Mp*rtn1*, and the MpRTN1-Citrine rescued line (Compl; Fig. 4C). Although no difference in ER branching was detected among lines, we observed a difference in tubule constriction. Analysis of binarized images clearly demonstrated that the ER tubules were thicker in Mp*rtn1* and thinner in Compl compared to the WT. The ER tubules in WT appeared as discontinuous lines, whereas the ER tubules in Mp*rtn1* showed clear continuity, suggesting reduced constriction due to the defect in MpRTN1. The ER tubules in Compl appeared narrowed and fragmented, which is similar to the phenotype when AtRTNs were overexpressed in Arabidopsis (Tolley *et al.*, 2008a; Sparkes *et al.*, 2010). We detected a significant difference in tubule diameter between WT and Mp*rtn1* or Compl (Fig. 4D). These results indicate that MpRTN1 plays an important role in constricting the ER membrane.

Mp*rtn1* shows a delayed chloroplast avoidance response

To analyze the functional relationship between Mpphot and MpRTN1, we examined the Mpphot-mediated chloroplast avoidance response, cold-avoidance response, and chloroplast accumulation response in WT, Mp*rtn1*, and Compl.

When the WT and Compl were irradiated with a strong blue microbeam at 22°C to induce the avoidance response, the chloroplasts began to move away from the irradiated area with a reaction time of a few minutes (Fig. 5A and 5B; Video S1 and S2). Mp*rtn1* showed a delay in the start of the avoidance response, with a reaction time of approximately 10 min (Fig. 5A and 5B; Video S3). To more accurately quantify the delay, we measured the time required to move the first 1 μm during the avoidance response. Chloroplasts in Mp*rtn1* required about 10 min more time to move the first 1 μm than in the WT and Compl (Fig. 5C).

We then investigated the cold avoidance response in the WT, Mp*rtn1*, and Compl. When WT cells were irradiated with weak white light at 5°C, the chloroplasts moved toward the anticlinal cell walls (Fig. 5D and 5E; Video S4 and S5). Similar to the avoidance response induced by strong blue light irradiation at 22°C, the chloroplasts took longer to start moving in Mp*rtn1* compared to the WT and Compl (Fig. 5D and 5E; Video S6). Chloroplasts in Mp*rtn1* required more time to move the first 1 μm than in the WT and Compl (Fig. 5F), and the distance of chloroplast movement at 240 min in Mp*rtn1* (approximately 2 μm) was nearly half that of the WT and Compl (approximately 4 μm) (Fig. 5E). These results suggest that MpRTN1 is required for rapid chloroplast movement during both the avoidance response and the cold-avoidance response.

We then assessed the chloroplast accumulation response. When the WT, Mp*rtn1*, and Compl were irradiated with a weak blue light microbeam at 22°C, the chloroplasts in these lines started to move toward the irradiated area with a reaction time of approximately 5 min (Fig. S3; Video S7, S8 and S9). The velocities of chloroplast movement were comparable in these lines, suggesting that MpRTN1 does not play a significant role in the chloroplast accumulation response.

Mp*rtn1* shows deformation of the ER structure during the chloroplast avoidance response

As MpRTN1 functions in ER tubule formation and cortical network maintenance, the delayed avoidance response and cold-avoidance response in Mp*rtn1* suggested that the ER is structurally related to chloroplast positioning. We thus observed changes in ER structure during the avoidance response by confocal microscopy. When WT or Compl cells were irradiated with 458-nm blue light, the ER structure changed in conjunction with chloroplast movement (Fig. 6A; Video S10 and S11). A mesh-like ER network was reformed in the gap between the chloroplasts that escaped from the irradiated area, and it appeared that the ER was restructured to facilitate chloroplast movement. By contrast, in Mp*rtn1*, stretched ER structures that were difficult to identify as tubules or sheets were observed following the avoidance response (Video S12). The space that formed between escaped chloroplasts in Mp*rtn1* contained more ER structures compared to the WT (Fig. 6B), suggesting that MpRTN1 is involved in the ER restructuring during the avoidance response. Taken together, these results suggest that MpRTN1 plays an important role in adjusting the ER structure to facilitate chloroplast movement during the avoidance response.

DISCUSSION

In this study, we provided several lines of evidence suggesting that the ER is restructured via the Mpphot-MpRTN1 interaction to facilitate chloroplast relocation movement. To our knowledge, this is the first report demonstrating the role of a phot interactor in the chloroplast avoidance response and an ER-resident protein in chloroplast movement.

During the avoidance response in Mp*rtn1*, the ER appeared to be abnormally stretched by the movement of chloroplasts escaping from blue light (Fig. 6A and 6B). This ER phenotype in Mp*rtn1* is likely due to the defect in the ER-restructuring activity of MpRTN1. We propose that in the WT, the ER that surrounds chloroplasts is restructured during the avoidance response so that the chloroplasts can move apart (Fig. 7). The aberrant ER stretching seen in the Mp*rtn1* mutant results from a defect in this ER restructuring, which generates an ER retraction force that counteracts the driving force for chloroplast separation. Consistent with our model, a previous study suggested that a *Drosophila* RTN is involved in ER remodeling and alleviates the retraction force of membrane tubule (Espadas *et al.*, 2019). In Arabidopsis, actin filaments associated with chloroplast (cp-actin) is thought to provide the driving force for chloroplast relocation (Kadota *et al.*, 2009). Chloroplasts may be able to move when the motive force provided by cp-actin exceeds the ER retraction force. Intriguingly, no delayed chloroplast accumulation response was observed in Mp*rtn1* (Fig. S3). A strong ER retraction force between chloroplasts is unlikely to occur during the accumulation response because chloroplasts do not move away from each other as they approach the light-irradiated area.

The cortical ER is in contact with the plasma membrane at intracellular subdomains known as the ER–plasma membrane contact sites (Prinz *et al.*, 2020). The BiFC analysis suggested that Mpphot interacts with MpRTN1 at these sites (Fig. 1C and Fig. 7). A previous study showed that human RTN3 is required to form a certain type of ER–plasma membrane contact sites (Caldieri *et al.*, 2017). MpRTN1 may function in the formation of ER–plasma membrane contact sites. Furthermore, an interactome study of RTNs in Arabidopsis (Kriechbaumer *et al.*, 2015) identified several proteins that localized to the plasma membrane and ER–plasma membrane contact sites as candidate RTN interactors. Remarkably, Atphot1 was included in the list of candidate RTN interactors (Kriechbaumer *et al.*, 2015). Therefore, the mechanisms of collaborative organelle repositioning by phot and RTN might be conserved in plants. However, in Arabidopsis cells, the ER network is constantly remodeled by cytoplasmic streaming, whereas Marchantia exhibits almost no cytoplasmic streaming (Era *et al.*, 2009). Therefore, Marchantia may have been significantly affected by the deficiency of ER restructure.

As it is unlikely that Mpphot and MpRTN1 always function as a complex, we propose that some signals are transduced from Mpphot to MpRTN1 (Fig. 7). Phot contains a kinase domain and transduces signals to several proteins via phosphorylation (Demarsy *et al.*, 2012; Takemiya *et al.*, 2013). However, in this study, phosphorylation of MpRTN1 was not detected (Fig. S1). There are two possible reasons for this. First, phosphorylation of MpRTN1 by Mpphot might be required for ER restructuring but at a level that is below the detection limit of immunoblot analysis. Non-phosphorylated MpRTN1 is abundant in the ER, and phosphorylated MpRTN1 might comprise only a small proportion of the MpRTN1 protein pool, even during the avoidance response. Second, the interaction between Mpphot and MpRTN1 might be indirect. The low recovery rate of MpRTN1 that co-immunoprecipitated with Mpphot (Fig. 1B) supports this notion. Mpphot might transduce a signal by phosphorylating a third factor that controls MpRTN1 activity to restructure the ER.

Most functional studies of AtRTNs in Arabidopsis have involved overexpression systems due to the redundancy of At*RTN* genes. When overexpressed, clade 1 AtRTNs induce ER tubule constriction (Sparkes *et al.*, 2010; Tolley *et al.*, 2008b; Tolley *et al.*, 2010), as was observed for MpRTN1 (Fig. 4C and 4D). Considering that MpRTN1 was classified in clade 1 together with other AtRTNs (Fig. 2), perhaps clade 1 RTNs evolved to play a major role in regulating the curvature of the ER membrane in plants. We also demonstrated that Marchantia, which has a lower level of genetic redundancy than other plants (Bowman *et al.*, 2017), contains five *RTN* genes (Fig. 2). Mp*rtn1* showed reduced ER tubule constriction and a delayed avoidance response, likely because unlike in Arabidopsis, there are no other clade 1 *RTN* genes in Marchantia that might compensate for the loss of MpRTN1 function (Fig. 4C, 4D and Fig.5). In addition to its low genetic redundancy, Marchantia exhibits almost no ER streaming, a rapid flow that frequently hinders live imaging analysis of ER dynamics in plant cells. Together, these features make Marchantia an attractive experimental material that is suitable for mutant analysis of ER morphology, dynamics, and function.

Plants cannot adjust to changing conditions by moving to another location. Instead, they respond to changing environments in part by controlling the intracellular positions of organelles (Islam *et al.*, 2009; Iwabuchi *et al.*, 2007; Oikawa *et al.*, 2015). Most of the plant cell volume is occupied by the vacuole (Winter *et al.*, 1994), and the cytoplasmic space in which other organelles can move is restricted. Therefore, organelles must move

cooperatively to achieve rapid and accurate positioning in response to the extracellular environment. Our findings provide evidence that plant cells adapt to fluctuating environments by controlling multiple organelle movements in a synchronized manner. Further studies are needed to elucidate the molecular mechanisms by which plant cells orchestrate organelle positioning and movement.

EXPERIMENTAL PROCEDURES

Plant materials and growth conditions

The gemmae of liverwort *M. polymorpha* were plated on one-half-strength B5 medium with 1% (w/v) agar and sucrose (without sucrose for analysis of chloroplast movement) and grown under continuous light (75 μmol photons $m^{-2} \cdot s^{-1}$) at 22°C. The Takaragaike-1 (Tak-1) accession was used as the wild type. For quantification of gemmaling growth, 10 gemmae were plated on the B5 medium, and this experiment was repeated three times. *N. benthamiana* was grown at 25°C under a 16-h-light/8-h-dark cycle in the soil (potting-mix:vermiculite = 1:3).

Plasmid construction and transformation

All primers used for PCR are listed in Table S1. To clone Mp*PHOT-3xFLAG*, the DNA fragments encoding *3xFLAG* were amplified by PCR using the 3xFLAG-F and FLAG-attB2 primers, which were designed to anneal to each other. The *3xFLAG* fragments were joined with DNA fragments encoding Mp*PHOT*, which were amplified by PCR using pENTR-Mpphot (Komatsu *et al.*, 2014) as a template, by recombinant PCR. The DNA fragments encoding Mp*RTN1* were amplified by PCR using a Tak-1 cDNA library as a template. The DNA fragments for the ER marker er-mCherry, which consists of mCherry flanked by the N-terminal signal peptide (25 amino acids) of field pumpkin (*Cucurbita pepo*) 2S albumin and the C-terminal ER retention signal sequence (HDEL) (Matsushima *et al.*, 2002), were amplified by two rounds of PCR. The first PCR was performed using pDONR207-mCherry (Osaki and Kodama, 2017) as a template, and the second PCR was performed using the product of the first PCR as a template. All PCR fragments described above were cloned into the pDONR207 vector using the Gateway BP reaction (Invitrogen). *MpPHOT* was cloned into the pDONR207 vector in a previous study (Kodama, 2016). These DNA fragments were then transferred by LR reaction (Invitrogen) to the destination vectors described below.

The Mp*PHOT* fragment was transferred to the pB4GWnY and pB4GWcY vectors, which are designed to express the cloned genes as the N-terminal half of YFP and the C-terminal half of YFP fusion proteins, respectively, under the control of the CaMV *35S* promoter (Kamigaki *et al.*, 2016). The Mp*PHOT-3xFLAG* fragment was transferred to the pGWB602 vector, which is designed to express the cloned genes under the control of the cauliflower mosaic virus (CaMV) *35S* promoter (Nakagawa *et al.*, 2007). The Mp*RTN1* fragment was transferred to the pGWB605, pMpGWB306, pB4GWnY, and pB4GWcY vectors, which are designed to express the cloned genes as GFP, Citrine, the N-terminal half of YFP, and the C-terminal half of YFP fusion proteins, respectively, under the control of the CaMV *35S* promoter (Nakagawa *et al.*, 2007; Ishizaki *et al.*, 2015; Kamigaki *et al.*, 2016). The *er-mCherry* fragment was transferred to the pMpGWB302 and pMpGWB402 vectors, which are designed to express the cloned genes under the control of the CaMV *35S* promoter (Ishizaki *et al.*, 2015). pMpGWB302-er-mCherry was used to generate transgenic Marchantia expressing er-mCherry in the Tak-1.

pMpGWB402-er-mCherry was used to generate transgenic Marchantia expressing er-mCherry in the Mp*rtn1* or Compl background. pGWB602Ω-CY, pB4GWnY-AtSYT1, and pB4GWcY-AtSYT1 were made in a previous study (Ishikawa *et al.*, 2020). The vector encoding the ER marker *er-GFP* was obtained from the Arabidopsis Biological Resource Center (stock number, CD3-955).

M. polymorpha plants were transformed using the AgarTrap method (Tsuboyama and Kodama, 2014; Tsuboyama *et al.*, 2018). Transgenic Marchantia expressing Citrine or Mpphot-Citrine was generated in a previous study (Tsuboyama and Kodama, 2014; Fujii *et al.*, 2017). The Mp*rtn1* mutant was generated by CRISPR/Cas9-mediated genome editing as described previously (Konno *et al.*, 2018). To generate a vector expressing the gRNA targeting Mp*RTN1*, two oligos (5′-CTCGTGTGGCGGAAGGAGCAGTGG-3′ and 5′-AAACCCACTGCTCCTTCCGCCACA-3′) were annealed and inserted into the pMpGE_En03 vector at the *Bsa*I site. The DNA fragment encoding the gRNA was transferred to the pMpGE010 vector, which is designed to express the gRNA together with CRISPR/Cas9 in Marchantia, by LR reaction (Sugano *et al.*, 2018).

Immunoprecipitation assay and mass spectrometry

The immunoprecipitation assay was performed with a μMACS GFP isolation kit (Miltenyi). We prepared 1 g of 7-day-old non-transgenic and transgenic Marchantia gemmalings expressing free Citrine or Mpphot-Citrine. All subsequent procedures were performed at 4°C. The gemmalings were ground in 3 mL extraction buffer [50 mM HEPES-KOH (pH 7.5), 0.3 M sucrose, 5 mM EDTA, 5 mM $MgCl_2$, 1 mM DTT, cOmplete, mini protease inhibitor cocktail (Roche)] with a mortar and pestle. The homogenate was centrifuged twice at 15,000 *g* for 10 min to remove the debris. After adding 50 μL Anti-Tag MicroBeads to the lysate, the wash and separation steps were performed according to the manufacturer's instructions.

The immunoprecipitates were separated by SDS-PAGE and digested into peptides for LC-MS/MS analysis as described previously (Fujiwara *et al.*, 2014). The spectra were compared with a protein database (Marchantia_v6.1) using the MASCOT server (version 2.7). The Mascot search parameters were as follows: threshold of the ion-score cut-off, 0.05; peptide tolerance, 10 ppm; MS/MS tolerance, ±0.8 Da; and peptide charge, 2+ or 3+. The search parameters allowed one missed cleavage by trypsin, a carbamidomethylation modification of cysteine residues, and a variable oxidation modification of methionine residues. The experiment was repeated twice; proteins that were specifically detected from the Mpphot-Citrine precipitates with a score > 100 in both biological replicates are listed in Fig. 1A. The scores of the first trial are shown in the list.

Co-immunoprecipitation and immunoblot analysis

Agrobacterium (*Rhizobium radiobacter*) strain GV2260 cells harboring pGWB602-MpPHOT-3xFLAG, pGWB605-MpRTN1, or the vector encoding *er-GFP* were cultured and resuspended in pure water to a final optical density of 1.0 at 600 nm. Equal volumes of Agrobacterium cultures were mixed and infiltrated into 4-week-old *N. benthamiana* leaves. All subsequent procedures were performed at 4°C. Two days after infiltration, two leaves were ground in 2 mL lysis buffer [50 mM Tris-HCl (pH 7.5), 150 mM $NaCl_2$, 0.5 mM EDTA, 0.5% (v/v) Nonidet P-40 (Sigma-Aldrich), cOmplete, mini protease inhibitor cocktail (Roche)] with a mortar and pestle. The homogenate was centrifuged at 15,000 *g*

for 10 min, and the supernatant was mixed with 40 µL Anti-DYKDDDDK tag antibody beads (Wako), followed by a 6-h rotation. The affinity beads were washed twice with 1 mL of lysis buffer. The proteins were eluted from the affinity beads by the addition of 40 µL of 2× Laemmli sample buffer (Bio-Rad). Immunoblot analysis was performed as described previously (Ishikawa *et al.*, 2015) with anti-DYKDDDDK (anti-FLAG) antibody (Wako), anti-GFP antibody (Roche), and anti-mouse secondary antibody (Thermo Fisher Scientific).

Bimolecular fluorescence complementation assay

Transformed Agrobacterium GV2260 cells harboring pB4GWnY-AtSYT1, pB4GWcY-AtSYT1, pB4GWnY-Mpphot, pB4GWcY-Mpphot, pB4GWnY-MpRTN1, pB4GWcY-MpRTN1, and pGWB602Ω-CY were cultured and infiltrated into *N. benthamiana* leaves as described above. Epidermal cells of abaxial leaves were observed by confocal microscopy two days after infiltration.

Immunoblot analysis of MpRTN1

The membrane-rich fraction was collected from 10-day-old gemmalings as described previously (Ishikawa *et al.*, 2015). A rabbit polyclonal antibody against MpRTN1 was generated using a synthetic peptide (NH2-C+IPRAAPKDKKAQ-COOH), corresponding to the C-terminal 12–amino acids of MpRTN1, as an antigen (Eurofins Genomics). For Phos-tag SDS-PAGE, we used 12-day-old gemmalings that were irradiated with blue light (50 µmol m^{-2} s^{-1}) for 30 min immediately before sample extraction. Phosphorylation of MpRTN1 was examined by Zn^{2+}-Phos-tag SDS-PAGE (Wako) (Kinoshita and Kinoshita-Kikuta, 2011) according to the manufacturer's instructions. Immunoblotting was performed as described above. Casein (2.5 µg) from milk (CAT# 07319-82; Nacarai Tesque) and dephosphorylated casein from bovine milk (CAT# 038-23221; Wako) were used as controls.

Confocal microscopy

Live-cell imaging was performed with an SP8X confocal microscope system (Leica Microsystems) equipped with HC PL APO CS 63× water-immersion lenses. Plant samples were mounted onto glass slides in pure water and covered with a coverslip. All images were taken in photon counting mode with the time-gating system (Kodama, 2016) at 100 Hz/1,024 × 1,024 pixels. Fluorescence intensities and ER tubule diameter were measured using Fiji (Schindelin *et al.*, 2012).

Analysis of chloroplast movement

Chloroplast movement was analyzed using a temperature-regulated microscope equipped with a microbeam irradiation system (Kato *et al.*, 2021; Tanaka *et al.*, 2017; Fujii *et al.*, 2017). Four-day-old gemmalings were used for the analysis. For the analysis of the accumulation response, 3-day-old gemmalings were cultured in the dark for 1 day to reduce the density of chloroplasts on the periclinal cell face by the induction of the dark positioning. Three chloroplasts within a cell were analyzed in three individual gemmalings. For the quantification of the time required to move the first 1 µm, chloroplasts whose final travel distance did not reach 1 µm were excluded. The chloroplast avoidance response was analyzed by confocal microscopy as follows. Three-day-old gemmalings were mounted onto glass slides in hydrogel (Hayashi *et al.*, 2017)

and covered with a coverslip as described previously (Sakata *et al.*, 2019). The edges of the coverslip were sealed with silicon to minimize focus drift. Images were taken in FRAP mode with photon counting and the time-gating system (Kodama, 2016) at 400 Hz/512 × 512 pixels. A FRAP cycle consisting of two frames (2.59 s) for blue laser irradiation and one frame (1.295 s) for post-irradiation was repeated 160 times. During the irradiation step, the region of interest was irradiated with a blue laser (458 nm, 0.2% intensity) from the argon laser source. During the post-irradiation steps, mCherry and chlorophyll autofluorescence were excited with 581-nm lasers from the white light laser source and detected at 592–658 nm and 670–680 nm with hybrid detectors, respectively. ER occupancy in the chloroplast gap was calculated using Fiji (Schindelin *et al.*, 2012). The chloroplast gap area was extracted with the create selection tool, and the area of the ER in the chloroplast gap was measured.

Database searching and phylogenetic analysis

RTN family genes in *M. polymorpha* were searched using MarpolBase MpTak v6.1 (https://marchantia.info/). The domain structures of RTNs were predicted using Pfam (http://pfam.xfam.org/). The amino acid sequences of reticulon domain were aligned and phylogenetically analyzed essentially as described previously (Ishikawa *et al.*, 2020). BLOSUM45 was used as a scoring matrix. The locus numbers and accession numbers are as follows: AtRTN1 (AT4G23630, NP001328059), AtRTN2 (At4G11220, NP192861), AtRTN3 (At1G64090, NP001185307), AtRTN4 (At5G41600, NP198975), AtRTN5 (At2G46170, NP566065), AtRTN6 (At3g61560, NP001319815), AtRTN7 (At4g01230, NP192032), AtRTN8 (At3g10260, NP850552), AtRTN9 (At3g18260, NP566604), AtRTN10 (At2g15280, NP179130), AtRTN11 (At3g19460, NP001325445), AtRTN12 (At3g54120, NP190980), AtRTN13 (At2g23640, NP565555), AtRTN14 (At1g68230, NP001117568), AtRTN15 (At2g01240, NP001318173), AtRTN16 (At3g10915, NP850557), AtRTN17 (At2g20590, NP179649), AtRTN18 (At4g28430, NP567809), AtRTN19 (At2g26260, NP180194), AtRTN20 (At2g43420, NP565998), AtRTN21 (At5g58000, NP001331115), MpRTN1 (Mp6g19200, PTQ41334), MpRTN2 (Mp6g19200, PTQ39501), MpRTN3 (Mp1g16900, OAE18363), MpRTN4 (Mp1g14200, PTQ27910), MpRTN5 (Mp1g17300, PTQ50009), and ScRTN1 (KOH51692).

ACCESSION NUMBERS

Accession numbers of genes analyzed in the present study are described in experimental procedures and figures.

DATA AVAILABILITY STATEMENT

Arabisopsis and Marchantia sequence data used in the present study were obtained from The Arabidopsis Information Resource (TAIR, https://www.arabidopsis.org/) and MarpolBase MpTak v6.1 (https://marchantia.info/), respectively. A RTN sequence of *Saccharomyces cerevisiae* were obtained from National Center for Biotechnology Information (NCBI, https://www.ncbi.nlm.nih.gov/). The transcriptome data for *M. polymorpha* was obtained from Bowman et al. (2017). The mass spectrometry proteomics data have been deposited to the ProteomeXchange Consortium via the PRIDE (Perez-Riverol *et al.*, 2022) partner repository with the dataset identifier PXD033077 and 10.6019/PXD033077. The data that support the findings of this study are available from the corresponding author upon reasonable request.

ACKNOWLEDGMENTS
We thank Ms. Hitomi Takahashi (Utsunomiya University) and Ms. Rie Kurata (Nara Institute of Science and Technology) for the technical assistance; Dr. Takayuki Kohchi (Kyoto University) for providing the *M. polymorpha* strains (Tak-1 and Mp*phot*^{KO}) and vectors (pMpGWB vector series, pMpGE_En03, and pMpGE010); Dr. Tsuyoshi Nakagawa (Shimane University) for providing vectors (pGWB602 and pGWB605); Dr. Shoji Mano (National Institute for Basic Biology) for providing vectors (pB4GWnY and pB4GWcY); and Dr. Takamasa Sakai (University of Tokyo) for providing the hydrogel. This work was supported by the Japan Science and Technology Agency Exploratory Research for Advanced Technology program (JST-ERATO; grant number JPMJER1602), JSPS KAKENHI (grant number 18H02455), and MEXT KAKENHI (grant numbers 20H05905 and 20H05910).

AUTHOR CONTRIBUTIONS
K.I., R.K., Y.F., and Y.K. conceived the research plans and performed most of the experiments including data analysis; M.F. and Y.F. performed mass spectrometry analysis; S.H. performed chloroplast movement analysis; Y.K. supervised the experiments; K.I. and Y.K. interpreted the results and wrote the manuscript with contributions from all authors.

CONFLICTS OF INTEREST
The authors declare that they have no conflicts of interest.

SUPPORTING INFORMATION LEGENDS
Figure S1. Phos-tag SDS-PAGE and immunoblot analysis of MpRTN1.

Figure S2. *RTN* genes in *M. polymorpha*.

Figure S3. Chloroplast accumulation response in Mp*rtn1*.

Table S1. Primers used in this study.

Video S1. (related to Fig. 5A) Chloroplast avoidance response in a WT gemmaling.

Video S2. (related to Fig. 5A) Chloroplast avoidance response in a Compl gemmaling.

Video S3. (related to Fig. 5A) Chloroplast avoidance response in an Mp*rtn1* gemmaling.

Video S4. (related to Fig. 5D) Chloroplast cold-avoidance response in a WT gemmaling.

Video S5. (related to Fig. 5D) Chloroplast cold-avoidance response in a Compl gemmaling.

Video S6. (related to Fig. 5D) Chloroplast cold-avoidance response in an Mp*rtn1* gemmaling.

Video S7. (related to Fig. S3A) Chloroplast accumulation response in a WT gemmaling.

Video S8. (related to Fig. S3A) Chloroplast accumulation response in an Mp*rtn1* gemmaling.

Video S9. (related to Fig. S3A) Chloroplast accumulation response in a Compl gemmaling.

Video S10. (related to Fig. 6A) ER dynamics during the chloroplast avoidance response in a WT gemmaling.

Video S11. (related to Fig. 6A) ER dynamics during the chloroplast avoidance response in a Compl gemmaling.

Video S12. (related to Fig. 6A) ER dynamics during the chloroplast avoidance response in an Mp*rtn1* gemmaling.

REFERENCES

Andersson, M.X., Gokso, M. and Sandelius, A.S. (2007) Optical manipulation reveals strong attracting forces at membrane contact sites between endoplasmic reticulum and chloroplasts. *J. Biol. Chem.*, **282**, 1170–1174.

Block, M.A. and Jouhet, J. (2015) Lipid trafficking at endoplasmic reticulum–chloroplast membrane contact sites. *Curr. Opin. Cell Biol.*, **35**, 21–29.

Bowman, J.L., Kohchi, T., Yamato, K.T., et al. (2017) Insights into land plant evolution garnered from the *Marchantia polymorpha* genome. *Cell*, **171**, 287–304.

Caldieri, G., Barbieri, E., Nappo, G., et al. (2017) Reticulon 3-dependent ER-PM contact sites control EGFR nonclathrin endocytosis. *Science (80-.).*, **356**, 617–624.

Demarsy, E., Schepens, I., Okajima, K., Hersch, M., Bergmann, S., Christie, J., Shimazaki, K.I., Tokutomi, S. and Fankhauser, C. (2012) Phytochrome Kinase Substrate 4 is phosphorylated by the phototropin 1 photoreceptor. *EMBO J.*, **31**, 3457–3467.

Era, A., Tominaga, M., Ebine, K., et al. (2009) Application of Lifeact Reveals F-Actin Dynamics in Arabidopsis thaliana and the Liverwort, Marchantia polymorpha. *Plant Cell Physiol.*, **50**, 1041–1048.

Espadas, J., Pendin, D., Bocanegra, R., et al. (2019) Dynamic constriction and fission of endoplasmic reticulum membranes by reticulon. *Nat. Commun.*, **10**, 1–11.

Fujii, Y., Ogasawara, Y., Takahashi, Y., Sakata, M., Noguchi, M., Tamura, S. and Kodama, Y. (2020) The cold-induced switch in direction of chloroplast relocation occurs independently of changes in endogenous phototropin levels. *PLoS One*, **15**, 1–15.

Fujii, Y., Tanaka, H., Konno, N., et al. (2017) Phototropin perceives temperature based on the lifetime of its photoactivated state. *Proc. Natl. Acad. Sci. U. S. A.*, **114**, 9206–9211.

Fujiwara, M., Uemura, T., Ebine, K., Nishimori, Y., Ueda, T., Nakano, A., Sato, M.H. and Fukao, Y. (2014) Interactomics of Qa-SNARE in *Arabidopsis thaliana*. *Plant Cell Physiol.*, **55**, 781–789.

Hayashi, K., Okamoto, F., Hoshi, S., et al. (2017) Fast-forming hydrogel with ultralow polymeric content as an artificial vitreous body. *Nat. Biomed. Eng.*, **1**, 1–7.

Hirano, S., Sasaki, K., Osaki, Y., Tahara, K., Takahashi, H., Takemiya, A. and Kodama, Y. (2022) The localization of phototropin to the plasma membrane defines a cold-sensing compartment in *Marchantia polymorpha*. *PNAS Nexus*, *pgac030.*

Huang, F.C. and Hwang, H.H. (2020) Arabidopsis reticulon-like4 (Rtnlb4) protein participates in agrobacterium infection and VirB2 peptide-induced plant defense response. *Int. J. Mol. Sci.*, **21**, 1722.

Ishikawa, K., Miura, C., Maejima, K., et al. (2015) Nucleocapsid protein from fig mosaic virus forms cytoplasmic agglomerates that are hauled by endoplasmic reticulum streaming. *J. Virol.*, **89**, 480–491.

Ishikawa, K., Tamura, K., Fukao, Y. and Shimada, T. (2020) Structural and functional relationships between plasmodesmata and plant endoplasmic reticulum-plasma membrane contact sites consisting of three synaptotagmins. *New Phytol.*, **226**, 798–808.

Ishikawa, K., Tamura, K., Ueda, H., Ito, Y., Nakano, A., Hara-Nishimura, I. and

Shimada, T. (2018) Synaptotagmin-associated endoplasmic reticulum-plasma membrane contact sites are localized to immobile ER tubules. *Plant Physiol.*, **178**, 641–653.

Ishizaki, K., Nishihama, R., Ueda, M., Inoue, K., Ishida, S., Nishimura, Y., Shikanai, T. and Kohchi, T. (2015) Development of gateway binary vector series with four different selection markers for the liverwort *Marchantia polymorpha*. *PLoS One*, **10**, e0138876.

Islam, M.S., Niwa, Y. and Takagi, S. (2009) Light-dependent intracellular positioning of mitochondria in *Arabidopsis thaliana* mesophyll cells. *Plant Cell Physiol.*, **50**, 1032–1040.

Iwabuchi, K., Sakai, T. and Takagi, S. (2007) Blue light-dependent nuclear positioning in *Arabidopsis thaliana* leaf cells. *Plant Cell Physiol.*, **48**, 1291–1298.

Jarillo, J.A., Gabrys, H., Capel, J., Alonso, J.M., Ecker, J.R. and Cashmore, A.R. (2001) Phototropin-related NPL1 controls chloroplast relocation induced by blue light. *Nature*, **410**, 952–954.

Kadota, A., Yamada, N., Suetsugu, N., et al. (2009) Short actin-based mechanism for light-directed chloroplast movement in Arabidopsis. *Proc. Natl. Acad. Sci. U. S. A.*, **106**, 13106–13111.

Kagawa, T., Sakai, T., Suetsugu, N., Oikawa, K., Ishiguro, S., Kato, T., Tabata, S., Okada, K. and Wada, M. (2001) *Arabidopsis* NPL1: a phototropin homolog controlling the chloroplast high-light avoidance response. *Science (80-.).*, **291**, 2138–2141.

Kamigaki, A., Nito, K., Hikino, K., Goto-Yamada, S., Nishimura, M., Nakagawa, T. and Mano, S. (2016) Gateway Vectors for Simultaneous Detection of Multiple Protein−Protein Interactions in Plant Cells Using Bimolecular Fluorescence Complementation P. K. Agarwal, ed. *PLoS One*, **11**, e0160717.

Kato, S., Takahashi, Y., Fujii, Y., Sasaki, K., Hirano, S., Okajima, K. and Kodama, Y. (2021) The photo-thermochemical properties and functions of Marchantia phototropin encoded by an unduplicated gene in land plant evolution. *J. Photochem. Photobiol. B Biol.*, **224**, 112305.

Kinoshita, E. and Kinoshita-Kikuta, E. (2011) Improved Phos-tag SDS-PAGE under neutral pH conditions for advanced protein phosphorylation profiling. *Proteomics*, **11**, 319–323.

Kinoshita, E., Kinoshita-Kikuta, E. and Koike, T. (2012) Phos-tag SDS-PAGE systems for phosphorylation profiling of proteins with a wide range of molecular masses under neutral pH conditions. *Proteomics*, **12**, 192–202.

Kinoshita, E., Kinoshita-Kikuta, E. and Koike, T. (2009) Separation and detection of large phosphoproteins using Phos-tag SDS-PAGE. *Nat. Protoc.*, **4**, 1513–1521.

Kiseleva, E., Morozova, K.N., Voeltz, G.K., Allen, T.D. and Goldberg, M.W. (2007) Reticulon 4a/NogoA locates to regions of high membrane curvature and may have a role in nuclear envelope growth. *J. Struct. Biol.*, **160**, 224–235.

Kodama, Y. (2016) Time gating of chloroplast autofluorescence allows clearer fluorescence imaging *in planta*. *PLoS One*, **11**, e0152484.

Kodama, Y., Suetsugu, N., Kong, S.-G. and Wada, M. (2010) Two interacting coiled-coil proteins, WEB1 and PMI2, maintain the chloroplast photorelocation movement velocity in *Arabidopsis*. *Proc. Natl. Acad. Sci. U. S. A.*, **107**, 19591–19596.

Kodama, Y., Tsuboi, H., Kagawa, T. and Wada, M. (2008) Low temperature-induced chloroplast relocation mediated by a blue light receptor, phototropin 2, in fern gametophytes. *J. Plant Res.*, **121**, 441–448.

Komatsu, A., Terai, M., Ishizaki, K., Suetsugu, N., Tsuboi, H., Nishihama, R., Yamato, K.T., Wada, M. and Kohchi, T. (2014) Phototropin encoded by a single-copy gene mediates chloroplast photorelocation movements in the *liverwort Marchantia* polymorpha. *Plant Physiol.*, **166**, 411–27.

Konno, R., Tanaka, H. and Kodama, Y. (2018) SKLPT imaging: Efficient *in vivo* pre-evaluation of genome-editing modules using fluorescent protein with peroxisome targeting signal. *Biochem. Biophys. Res. Commun.*, **503**, 235–241.

Kriechbaumer, V., Botchway, S.W., Slade, S.E., Knox, K., Frigerio, L., Oparka, K. and Hawes, C. (2015) Reticulomics: Protein-protein interaction studies with two plasmodesmata-localized reticulon family proteins identify binding partners enriched at plasmodesmata, endoplasmic reticulum, and the plasma membrane. *Plant Physiol.*, **169**, 1933–1945.

Kriechbaumer, V., Maneta-Peyret, L., Fouillen, L., et al. (2018) The odd one out: *Arabidopsis* reticulon 20 does not bend ER membranes but has a role in lipid regulation. *Sci. Rep.*, **8**, 2310.

Lazareva, E.A., Lezzhov, A.A., Chergintsev, D.A., Golyshev, S.A., Dolja, V. V., Morozov, S.Y., Heinlein, M. and Solovyev, A.G. (2021) Reticulon-like properties of a plant virus-encoded movement protein. *New Phytol.*, **229**, 1052–1066.

Matsushima, R., Hayashi, Y., Kondo, M., Shimada, T., NISHIMURA, M. and Hara-Nishimura, I. (2002) An endoplasmic reticulum-derived structure that is induced under stress conditions in Arabidopsis. *Plant Physiol.*, **130**, 1807–1814.

Nakagawa, T., Suzuki, T., Murata, S., et al. (2007) Improved gateway binary vectors: High-performance vectors for creation of fusion constructs in transgenic analysis of plants. *Biosci. Biotechnol. Biochem.*, **71**, 2095–2100.

Nziengui, H., Bouhidel, K., Pillon, D., Der, C., Marty, F. and Schoefs, B. t (2007) Reticulon-like proteins in *Arabidopsis thaliana*: Structural organization and ER localization. *FEBS Lett.*, **581**, 3356–3362.

Oikawa, K., Matsunaga, S., MANO, S., et al. (2015) Physical interaction between peroxisomes and chloroplasts elucidated by *in situ* laser analysis. *Nat. Plants*, **1**, 15012–15035.

Oikawa, K., Yamasato, A., Kong, S.-G., Kasahara, M., Nakai, M., Takahashi, F., Ogura, Y., Kagawa, T. and Wada, M. (2008) Chloroplast outer envelope protein CHUP1 is essential for chloroplast anchorage to the plasma membrane and chloroplast movement. *Plant Physiol.*, **148**, 829–42.

Osaki, Y. and Kodama, Y. (2017) Particle bombardment and subcellular protein localization analysis in the aquatic plant *Egeria densa*. *PeerJ*, **5**, e3779.

Perez-Riverol, Y., Bai, J., Bandla, C., et al. (2022) The PRIDE database resources in 2022: A hub for mass spectrometry-based proteomics evidences. *Nucleic Acids Res.*, **50**, D543–D552.

Prinz, W.A., Toulmay, A. and Balla, T. (2020) The functional universe of membrane contact sites. *Nat. Rev. Mol. Cell Biol.*, **21**, 7–24.

Sakai, T., Kagawa, T., Kasahara, M., Swartz, T.E., Christie, J.M., Briggs, W.R., Wada, M. and Okada, K. (2001) *Arabidopsis* nph1 and npl1: blue light receptors

that mediate both phototropism and chloroplast relocation. *Proc. Natl. Acad. Sci.*, **98**, 6969–6974.

Sakata, M., Kimura, S., Fujii, Y., Sakai, T. and Kodama, Y. (2019) Relationship between relocation of phototropin to the chloroplast periphery and the initiation of chloroplast movement in *Marchantia polymorpha*. *Plant Direct*, **3**, e00160--13.

Schindelin, J., Arganda-Carreras, I., Frise, E., et al. (2012) Fiji: an open-source platform for biological-image analysis. *Nat. Methods*, **9**, 676–682.

Sparkes, I., Tolley, N., Aller, I., Svozil, J., Osterrieder, A., Botchway, S., Mueller, C., Frigerio, L. and Hawes, C. (2010) Five *Arabidopsis* reticulon isoforms share endoplasmic reticulum location, topology, and membrane-shaping properties. *Plant Cell*, **22**, 1333–1343.

Suetsugu, N. and Wada, M. (2020) Signalling mechanism of phototropin-mediated chloroplast movement in Arabidopsis. *J. Plant Biochem. Biotechnol.*, **29**, 580–589.

Suetsugu, N., Yamada, N., Kagawa, T., Yonekura, H., Uyedad, T.Q.P., Kadota, A. and Wada, M. (2010) Two kinesin-like proteins mediate actin-based chloroplast movement in *Arabidopsis thaliana*. *Proc. Natl. Acad. Sci. U. S. A.*, **107**, 8860–8865.

Sugano, S.S., Nishihama, R., Shirakawa, M., et al. (2018) Efficient CRISPR/Cas9-based genome editing and its application to conditional genetic analysis in *Marchantia polymorpha*. *PLoS One*, **13**, e0205117.

Takemiya, A., Sugiyama, N., Fujimoto, H., Tsutsumi, T., Yamauchi, S., Hiyama, A., Tada, Y., Christie, J.M. and Shimazaki, K. (2013) Phosphorylation of BLUS1 kinase by phototropins is a primary step in stomatal opening. *Nat. Commun.*, **4**, 2094.

Tanaka, H., Sato, M., Ogasawara, Y., Hamashima, N., Buchner, O., Holzinger, A., Toyooka, K. and Kodama, Y. (2017) Chloroplast aggregation during the cold-positioning response in the liverwort *Marchantia polymorpha*. *J. Plant Res.*, **130**, 1061–1070.

Tolley, N., Sparkes, I., Craddock, C.P., Eastmond, P.J., Runions, J., Hawes, C. and Frigerio, L. (2010) Transmembrane domain length is responsible for the ability of a plant reticulon to shape endoplasmic reticulum tubules *in vivo*. *Plant J.*, **64**, 411–418.

Tolley, N., Sparkes, I.A., Hunter, P.R., Craddock, C.P., Nuttall, J., Roberts, L.M., Hawes, C., Pedrazzini, E. and Frigerio, L. (2008a) Overexpression of a plant reticulon remodels the lumen of the cortical endoplasmic reticulum but does not perturb protein transport. *Traffic*, **9**, 94–102.

Tolley, N., Sparkes, I.A., Hunter, P.R., Craddock, C.P., Nuttall, J., Roberts, L.M., Hawes, C., Pedrazzini, E. and Frigerio, L. (2008b) Overexpression of a plant reticulon remodels the lumen of the cortical endoplasmic reticulum but does not perturb protein transport. *Traffic*, **9**, 94–102.

Tsuboyama, S. and Kodama, Y. (2014) AgarTrap: A simplified *Agrobacterium*-mediated transformation method for sporelings of the liverwort *Marchantia polymorpha* L. *Plant Cell Physiol.*, **55**, 229–236.

Tsuboyama, S., Nonaka, S., Ezura, H. and Kodama, Y. (2018) Improved G-AgarTrap: A highly efficient transformation method for intact gemmalings of the liverwort *Marchantia polymorpha*. *Sci. Rep.*, **8**, 10800.

Voeltz, G.K., Prinz, W.A., Shibata, Y., Rist, J.M. and Rapoport, T.A. (2006) A

class of membrane proteins shaping the tubular endoplasmic reticulum. *Cell*, **124**, 573–586.

Wada, M. (2013) Chloroplast movement. *Plant Sci.*, **210**, 177–182.

Wang, P., Hawes, C. and Hussey, P.J. (2017) Plant endoplasmic reticulum-plasma membrane contact sites. *Trends Plant Sci.*, **22**, 289–297.

Winter, H., Robinson, D.G. and Heldt, H.W. (1994) Subcellular volumes and metabolite concentrations in spinach leaves. *Planta*, **193**, 530–535.

Zhang, H. and Hu, J. (2016) Shaping the endoplasmic reticulum into a social network. *Trends Cell Biol.*, **26**, 934–943.

Zhang, X., Ding, X., Marshall, R.S., Paez-Valencia, J., Lacey, P., Vierstra, R.D. and Otegui, M.S. (2020) Reticulon proteins modulate autophagy of the endoplasmic reticulum in maize endosperm. *Elife*, **9**, 1–27.

FIGURES

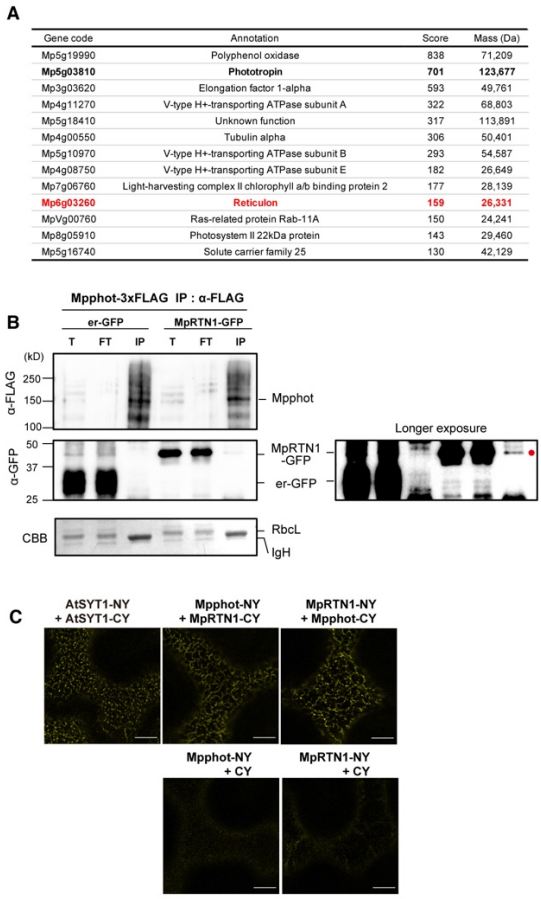

Figure 1. Identification of MpRTN1 as an Mpphot interactor.
(A) Identification of Mpphot-interacting proteins by immunoprecipitation with Mpphot-Citrine and mass spectrometry. Mpphot is indicated in bold. *Marchantia polymorpha* RETICULON1 (MpRTN1) is shown in red font. (B) Co-immunoprecipitation of Mpphot-3xFLAG and MpRTN1-GFP with an anti-FLAG antibody. Immunoprecipitation experiments were performed using *N. benthamiana* leaves expressing Mpphot-3xFLAG and GFP-HDEL or MpRTN1-GFP. T, total fraction; FT, flow-through fraction; IP, immunoprecipitated sample. Coomassie Brilliant Blue (CBB) staining shows blots of Rubisco large subunits (RbcL) and immunoglobulin heavy chain (IgH) detached from the matrix of affinity beads as a loading control. An image captured with a longer exposure time is provided to clearly indicate the MpRTN1-GFP band in the immunoprecipitated sample (red dot). (C) Bimolecular fluorescence complementation (BiFC) assay. AtSYT1, Mpphot, and MpRTN1 fused with the N-terminal half of YFP (AtSYT1-, Mpphot-, and MpRTN1-NY) was transiently expressed with AtSYT1, Mpphot, MpRTN1 fused with the C-terminal half of YFP (AtSYT1-, Mpphot-, MpRTN1-CY), or free C-terminal half of YFP (CY) in *N. benthamiana* leaves. Bars = 10 μm.

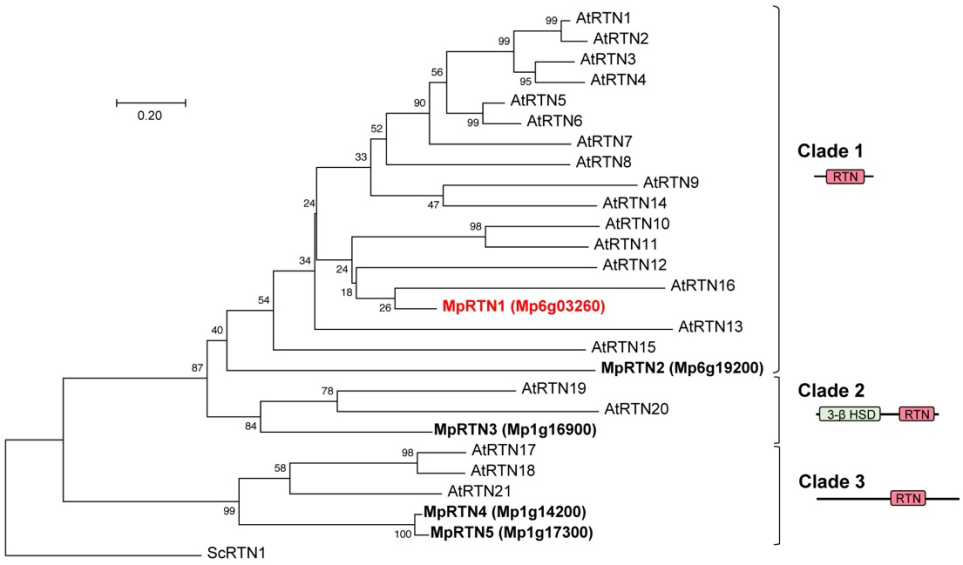

Figure 2. Phylogenetic analysis of Arabidopsis and Marchantia RTNs.
A maximum likelihood phylogenetic tree of Arabidopsis and Marchantia RTNs using the RTN domain. Bootstrap values (%) are listed next to each node. Marchantia RTNs and MpRTN1 are shown in bold and red text, respectively. An RTN of *Saccharomyces cerevisiae* (ScRTN1) was used as an outgroup. The schematic diagram shows the putative domain structures of RTNs in each class. RTN, reticulon domain; 3β HSD, 3-beta hydroxysteroid dehydrogenase/isomerase family domain.

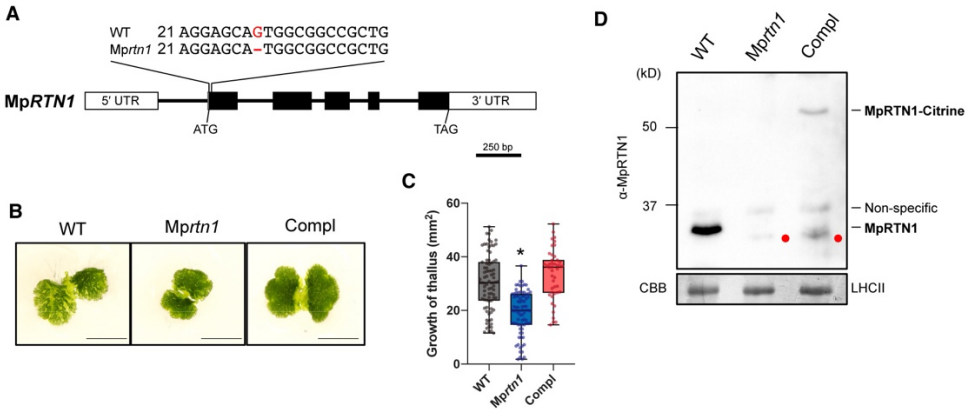

Figure 3. Generation of a Marchantia mutant deficient in MpRTN1.
(A) The gene structure of Mp*RTN1*. Boxes indicate exons (black) and 5′ and 3′ UTRs (white). Nucleotide alignments showing the mutation introduced in Mp*rtn1*. (B) Ten-day-old WT, Mp*rtn1*, and Compl gemmalings. Bars = 1 mm. (C) Quantification of thallus growth. $n = 30$; horizontal lines in the middle of each box plot represent median values; asterisks indicate significant difference from the WT, $P < 0.05$, using Tukey's multiple comparisons test. (D) Immunoblot of the WT, Mp*rtn1*, and Mp*rtn1* expressing MpRTN1-Citrine (Compl) using an anti-MpRTN1 antibody. Red dots indicate a truncated form MpRTN1. Coomassie Brilliant Blue (CBB) staining of blots of light-harvesting complex II (LHCII) was performed as a loading control.

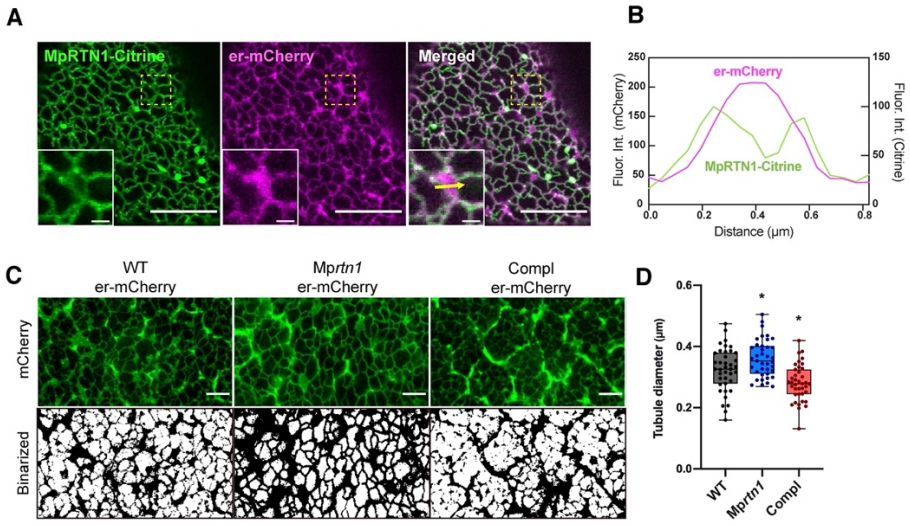

Figure 4. MpRTN1 plays a role in regulating curvature of the ER membrane.
(A) Localization of MpRTN1-Citrine at the ER. Three-day-old gemmalings expressing the ER marker er-mCherry in the rescued line background (Compl) were analyzed by confocal microscopy. Insets show detailed views of the ER sheet indicated by dashed yellow squares. Bars = 5 μm and 0.5 μm (inset). (B) Fluorescence intensities of Citrine and mCherry along the yellow arrow crossing a sheet shown in the inset of (A). (C) ER morphology of the WT, Mp*rtn1*, and Compl. Three-day-old gemmalings expressing the ER marker er-mCherry in the WT, Mp*rtn1*, and Compl backgrounds were analyzed by confocal microscopy. Lower panels show binarized images of the confocal images. Bars = 5 μm. (D) Quantification of tubule diameter. $n = 39$; horizontal lines in the middle of each box plot represent median values; asterisks indicate significant difference from the WT, $P < 0.05$, using Dunnett's multiple comparison test.

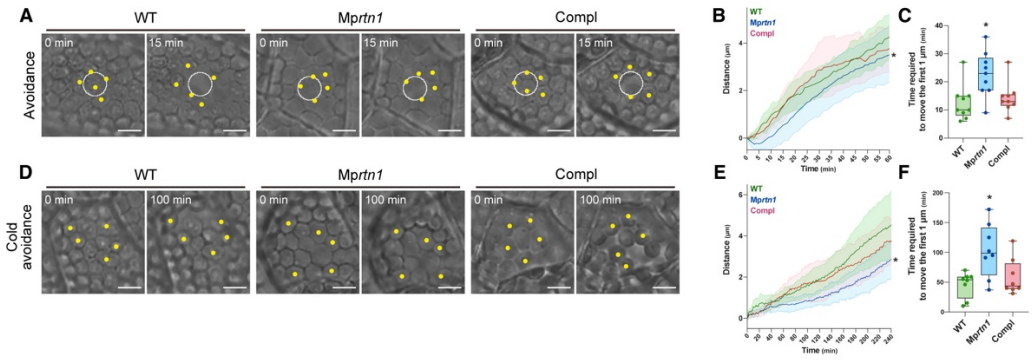

Figure 5. The Mp*rtn1* mutant displays a delayed chloroplast avoidance response.
(A and D) Chloroplast avoidance response (A) and cold-avoidance response (D) in 4-day-old WT, Mp*rtn1*, and Compl (Mp*rtn1* expressing MpRTN1-Citrine) gemmalings. The areas in the white circles were irradiated with blue beams (100 W m^{-2}) in (A). The cells were irradiated with white light (140 μmol m^{-2} s^{-1}) at 5°C in (D). Yellow dots indicate chloroplast positions. Bars = 10 μm. (B and E) Quantification of chloroplast avoidance response (B) and cold-avoidance response (E). The distance from the center of the white circle (blue-beam-irradiated area) to the chloroplasts was quantified in (B). The distance traveled from the first position of the chloroplasts (d) was quantified in (E). $n = 9$; colored solid lines and areas show the mean distance and standard deviations (± SD) for WT (green), Mp*rtn1* (blue), and Compl (red), respectively; asterisks indicate significant difference from the WT in the range of $10 \leqq t$ (time) $\leqq 12$ (B), $16 \leqq t \leqq 19$ (B), and $105 \leqq t$ (E); $P < 0.05$, using Dunnett's multiple comparison test. (C and F) Quantification of time required to move the first 1 μm in chloroplast avoidance response (C) and cold-avoidance response (F). The same datasets as (B and E) were used. Horizontal lines in the middle of each box plot represent median values. n = 8 or 9; asterisks indicate significant difference from the WT, $P < 0.05$, using Dunnett's multiple comparison test.

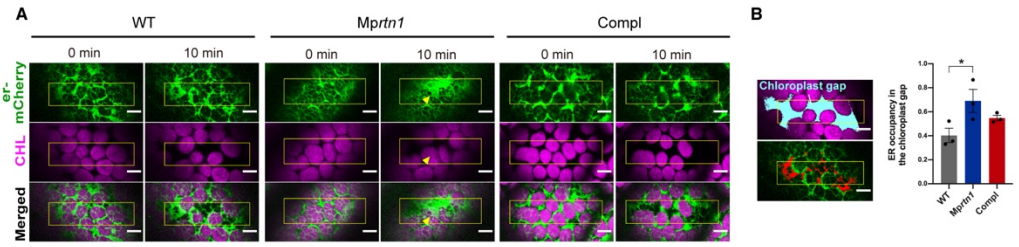

Figure 6. The maintenance of ER structure during chloroplast avoidance response was impaired in the Mp*rtn1* mutant.
Structural changes in the ER during chloroplast avoidance movement in 3-day-old gemmalings expressing the ER marker er-mCherry in WT, Mp*rtn1*, and Compl backgrounds. (A) Confocal microscopy of gemmaling cells. The areas indicated by yellow rectangles were irradiated with blue light (458 nm). er-mCherry is pseudo-colored in green, and chlorophyll autofluorescence of chloroplasts is colored in magenta (CHL). Yellow arrowheads indicate an aberrant ER structure formed in a gap between chloroplasts. Bars = 5 μm. (B) Quantification of ER occupancy in a chloroplast gap. Left upper and lower panels show a chloroplast gap (colored in cyan) and ER in the chloroplast gap (colored in red), respectively. WT cells 10 min after blue light irradiation were used for the images. n = 3; data are shown as means ± SD; asterisks indicate significant difference from the WT, $P < 0.05$, using Student's t-test.

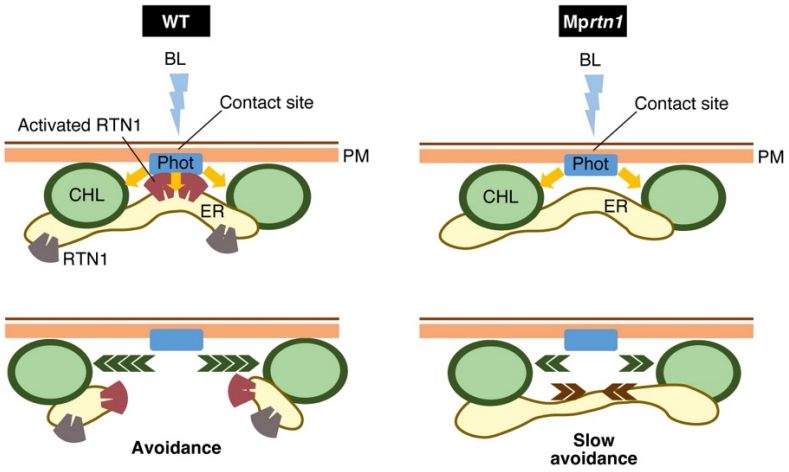

Figure 7. A model for collaborative organelle repositioning by phot and RTN in *Marchantia polymorpha.*
In WT cells, Mpphot on the plasma membrane (PM) and MpRTN1 in the ER membrane interact at ER–plasma membrane contact sites. Mpphot perceives blue light (BL) and transduces the signal (yellow arrows) to both MpRTN1 and chloroplasts (CHL). The ER network is restructured by MpRTN1 that had been activated by Mpphot signaling, in conjunction with chloroplast avoidance movement (green chevron arrows). In Mp*rtn1* cells, lack of MpRTN1 leads to insufficient ER restructuring during the chloroplast avoidance response and prevents rapid chloroplast movement by generating a counteracting force against the movement of chloroplasts (brown chevron arrows).

Fig. S1 Ishikawa et al.

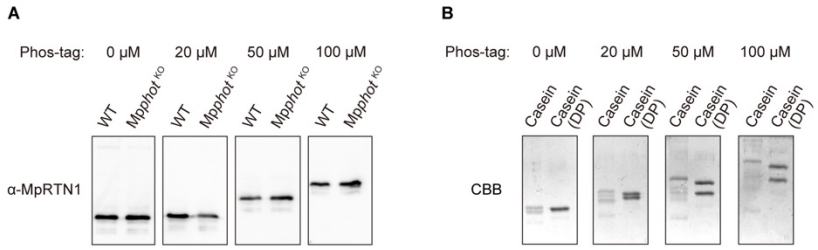

Figure S1. Phos-tag SDS-PAGE and immunoblot analysis of MpRTN1.

(A) WT and Mp*phot*^{KO} gemmalings irradiated with blue light (50 μmol m^{-2} s^{-1}) were analyzed by immunoblotting with Phos‐tag SDS-PAGE and anti-MpRTN1 antibody. Membrane-rich fractions from both types of plants were separated by electrophoresis on polyacrylamide gels with various concentrations of Phos‐tag (0, 20, 50, and 100 μM). (B) Phos-tag SDS-PAGE of caseins as a control. DP indicates commercial dephosphorylated casein, which contains a dephosphorylated form and a phosphorylated form. Gels were stained with Coomassie Brilliant Blue (CBB).

Fig. S2 Ishikawa et al.

					antheridiophore	archegoniophore	sporophyte	sporeling	thallus
gene id		gene	nt length	aa length	FPKM	FPKM	FPKM	FPKM	FPKM
Mapoly0035s0106	Mp6g03260	Mp*RTN1*	1687	243	13.2663	53.2242	16.0762	9.52989	9.34211
Mapoly0045s0143	Mp6g19200	Mp*RTN2*	1973	192	3.99688	5.58671	6.19975	4.33132	7.19266
Mapoly0001s0030	Mp1g16900	Mp*RTN3*	2520	569	42.1919	35.9472	49.3269	48.8376	32.8587
Mapoly0179s0001	Mp1g14200	Mp*RTN4*	2895	640	58.8408	36.0093	58.9317	13.149	3.31241
Mapoly0001s0070	Mp1g17300	Mp*RTN5*	1354	189	25.8497	6.68336	2.00154	0.0527427	3.61072

Figure S2. *RTN* genes in *M. polymorpha*.
Gene expression data are based on a study by Bowman et al. (28).

Fig. S3 Ishikawa et al.

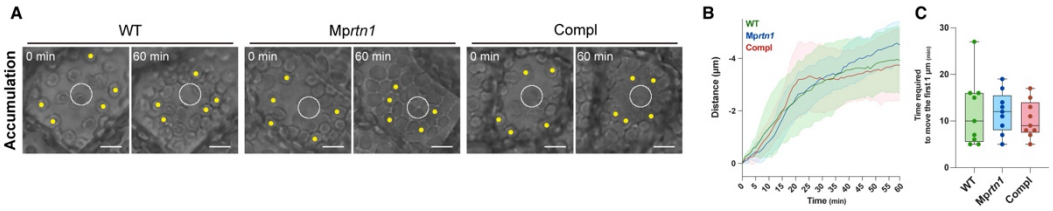

Figure S3. Chloroplast accumulation response in Mp*rtn1*.

(A) Chloroplast accumulation response in 4-day-old WT, Mp*rtn1*, and Compl gemmalings. The areas in white circles were irradiated with blue light (10 W m^{-2}). Yellow dots indicate changes in chloroplast positions. (B) Quantification of the distance from the center of the white circle (blue beam irradiated area) to the chloroplasts was quantified. $n = 9$; colored solid lines and areas show the mean distance and standard deviations (± SD) for WT (green), Mp*rtn1* (blue), and Compl (red), respectively. (C) Quantification of time required to move the first 1 µm. The same datasets as (B) were used. $n = 9$; horizontal lines in the middle of each box plot represent median values.

Table S1

Name	Primer seqence (5′–3′)
3xFLAG-F	GTGGTTGATAACAGCGATTACAAGGATGACGATGACAAGGATTACAAGGATGACGATGACAAGGATTACAAGGATGACGATGACAAGTGATTAAATAGAA
FLAG-attB2	GGGGACCACTTTGTACAAGAAAGCTGGGTCTTTCTATTTAATCACTTGT
PHOT-attB1	GGGGACAAGTTTGTACAAAAAAGCAGGCTTCATGATGCCCTCCACGGAT
PHOT-FLAG-R	GCTGTTATCAACCACATATTCATCAAATGA
RTN-attb1	GGGGACAAGTTTGTACAAAAAAGCAGGCTTCATGTCTGAACATGTGGCG
RTN-attb2	GGGGACCACTTTGTACAAGAAAGCTGGGTCCTGCGCCTTCTTGTCCTTG
SP-mCherry-F	TTGCCCTCTTCGCAGTGGCTCTGCTGGTTGCAGATGCGTACGCCTACCGCACAATGGTGAGCAAGGGCGA
mCherry-HDEL-attb2	GGGGACCACTTTGTACAAGAAAGCTGGGTCCTAGAGCTCGTCGTGCTTGTACAGCTCGTC
SP-mCherry-attB1	GGGGACAAGTTTGTACAAAAAAGCAGGCTTCATGGCCAGACTCACAAGCATCATTGCCCTCTTCGCAGTG